Palaeogeography, Palaeoclimatology, Palaeoecology 631 (2023) 111834

Contents lists available at ScienceDirect

Palaeogeography, Palaeoclimatology, Palaeoecology

journal homepage: www.elsevier.com/locate/palaeo

# Laguna Seca sediments reveal environmental and climate change during the latest Pleistocene and Holocene in Sierra Nevada, southern Iberian Peninsula

Gonzalo Jiménez-Moreno [a,*], Alejandro López-Avilés [a], Antonio García-Alix [a,b], María J. Ramos-Román [c], Jon Camuera [b], Jose Manuel Mesa-Fernández [a], Francisco J. Jiménez-Espejo [b], Charo López-Blanco [a], José S. Carrión [d], R. Scott Anderson [e]

[a] Departamento de Estratigrafía y Paleontología, Universidad de Granada, Spain
[b] Instituto Andaluz de Ciencias de la Tierra (IACT), CSIC-UGR, Armilla, Spain
[c] Facultad de Educación, Universidad del Atlántico Medio, Madrid, Spain
[d] Department of Plant Biology, Faculty of Biology, University of Murcia, Spain
[e] School of Earth and Sustainability, Northern Arizona University, USA

ARTICLE INFO

Editor: M Elliot

*Keywords:*
Vegetation
Lake level
Climate
Late Pleistocene
Holocene
Western Mediterranean

ABSTRACT

Sedimentation in most glacial lakes and wetlands in the Sierra Nevada (southern Iberian Peninsula) began after the last deglaciation and since the Younger Dryas (YD)-Early Holocene (EH) transition. Therefore, until now, studies on older sedimentary records were lacking in this alpine area, which limits the paleoenvironmental and paleoclimatic information to the Holocene. In this study, we studied palynomorphs from the alpine record from Laguna Seca (LS), the longest and oldest (~18,000 cal yr BP = 18 kyr) sedimentary record in the Sierra Nevada to investigate the response of forests and lake environments in the western Mediterranean area to climate changes and human impact during the latest Pleistocene and Holocene. The deepest lake conditions occurred during the last deglaciation, indicated by the occurrence of *Pediastrum* algae, which showed highest abundances during the Heinrich Stadial 1 (HS1) and Bølling-Allerød (B-A) transition. Xerophyte herbs such as *Artemisia*, *Ephedra*, and Amaranthaceae were highest during the late B-A and YD indicating regional aridity. Poaceae (grasses) were maxima in the B-A and EH, probably indicating expansion in the barren areas after deglaciation. Maximum in temperature and humidity during the EH and cooling and aridification in the Middle (MH) and Late Holocene (LH) are indicated by the changes in the abundance of deciduous *Quercus* and *Pinus* forest species. *Botryococcus* algae increased during the Early Holocene, while the rest of the algae almost vanished, which could indicate that the lake became very productive but shallower until 8.2 kyr. The lake level lowered and became seasonal in the Middle-Late Holocene transition, coinciding with the regional climate aridification. Microcharcoal analysis done on the palynological preparations agrees with the vegetation changes, showing maxima in the EH and MH, related with the maximum in regional forest occurrence, and a decrease in the LH when the Mediterranean vegetation, and thus fuel availability, diminished. This record shows evidence of anthropogenic impact in the last centuries by cultivation, reforestation, cattle grazing, enhanced erosion and eutrophication.

## 1. Introduction

The Sierra Nevada is one of the highest elevation and southernmost-located mountain range in southern Europe (Fig. 1). It lies within a particular biogeographic region (Zamora and Oliva, 2022), renowned as a biodiversity super hotspot (Arroyo et al., 2022). High-elevation mountain environments can be particularly sensitive to recent climate warming and increase in drought conditions (Páscoa et al., 2017), which is causing altitudinal displacements of plant and animal species, and loss of biodiversity in the Sierra Nevada (Lorite et al., 2022). With projections of annual mean warming on land of 0.9–5.6 °C at the end of the century in the Mediterranean area (Ali et al., 2022), what will be the environmental consequences of such a rapid climate change in mountains such as the Sierra Nevada?

* Corresponding author.
*E-mail address:* gonzaloj@ugr.es (G. Jiménez-Moreno).

https://doi.org/10.1016/j.palaeo.2023.111834
Received 20 April 2023; Received in revised form 11 July 2023; Accepted 2 October 2023
Available online 5 October 2023

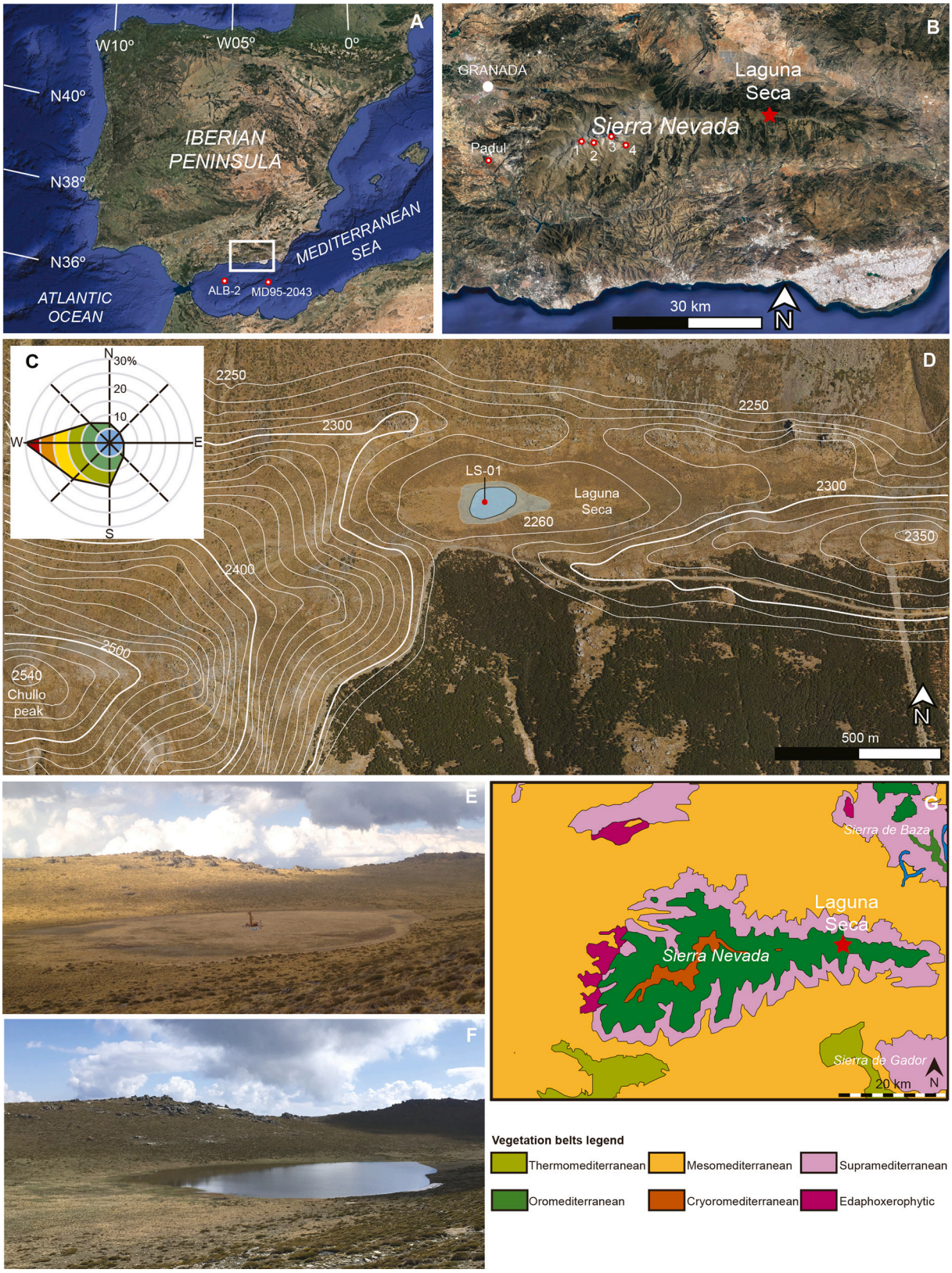


**Fig. 1.** (A) Location of Sierra Nevada (rectangle) within the Iberian Peninsula, western Mediterranean region. The MD95–2043 and ALB-2 marine sites discussed in the text are also shown. Satellite photo from Google Earth. (B) Location of Laguna Seca (LS) within the Sierra Nevada. The Padul and Sierra Nevada sites discussed in the text are also shown (1: Borreguil de la Virgen; 2: Laguna de Río Seco; 3: Laguna de la Mosca; 4: Laguna Hondera). Satellite photo from Google Earth. (C) Wind direction in percentage from January 2000 to December 2019 for Granada, Spain (data obtained from https://www.woeurope.eu) (D) LS area and topography. Note the treeline immediately south of the lake at ~2300 m. Satellite photo from Google Earth. (E) LS during the coring of LS-01 in September 2014. (F) LS containing water in early June 2018. (G) Map of the vegetation belts in the Sierra Nevada (Modified from REDIAM. Map of the vegetation series of Andalucía: http://laboratoriorediam.cica.es/VisorGenerico/?tipo=WMS). Figure modified from Ramos-Román et al. (2018a) and López-Avilés et al. (2022).

Paleoecological and paleoclimatic studies are necessary to predict the future, improving our understanding of the relationship between climate and mountain ecosystems in the past, especially during warmer and drier periods than at present and during significant climatic fluctuations such as the glacial-interglacial transitions. In this respect, there are more than 50 small glacial-origin alpine lakes and bogs in the Sierra Nevada that accumulated sediments preserving a high-quality signal of past natural and anthropogenic environmental and climate change (Anderson et al., 2011; Jiménez-Moreno and Anderson, 2012; García-Alix et al., 2012, 2013, 2017, 2018, 2020; Jiménez-Espejo et al., 2014; Jiménez-Moreno et al., 2013, 2020; Ramos-Román et al., 2016, 2018a, 2018b, 2019; Mesa-Fernández et al., 2018; Manzano et al., 2019; Toney et al., 2020; López-Avilés et al., 2021; Alba-Sánchez et al., 2021). Previous studies show that in the glacial lakes and wetlands from the Sierra Nevada sedimentation started after deglaciation and thereafter since the Early Holocene (see synthesis in Jiménez-Moreno et al., 2022). Therefore, older sedimentary records were yet to be found in this alpine area to widen our knowledge about environmental change further in time and since the last deglaciation.

In 2014 three sedimentary cores, LS-01, LS-02 and LS-03, were obtained from LS (López-Avilés et al., 2022; Fig. 1), still in the alpine area but at lower elevation than the previous studies. The age model for the 14 m-long sedimentary sequence, based on nine Accelerator Mass Spectometry (AMS) radiocarbon and four optically stimulated luminescence (OSL) dates, shows a continuous record of the last ~18 kyr and since the Last Glacial Maximum (LGM) (López-Avilés et al., 2022; Fig. 2). In this study, we analyzed palynomorphs and charcoal abundance from the LS-01 alpine record, which represents so far, the longest and oldest sedimentary record in Sierra Nevada, southern Spain. Our goal is to document vegetational developments through palynological and charcoal data and join those to previously reported chronological, sedimentological and geochemical information by López-Avilés et al. (2022). Furthermore, the comparison of the LS-01 record with detailed paleoenvironmental and paleoclimatic records from the western Mediterranean allows us to obtain information on potential climatic and anthropogenic triggers for past environmental change in the study area.

## 2. Study site

LS (37° 05′ 53”N, 2° 58′ 05”W, 2259 m above sea level) is a small endorheic alpine lake basin located in the eastern sector of the Sierra Nevada facing south right below the ridge line (Fig. 1). LS formed from the combination of tectonics, including a rotational fault, and subsequent glacial and periglacial erosion, indicated by the occurrence of moraines in the LS valley (Simón et al., 2000). At present, LS gets covered with ice and snow in winter and becomes inundated in spring and early summer, when the lake level can be as high as 50 cm (personal observations between 2014 and 2023). LS is seasonally dry during summer and early fall (Fig. 1). The lake water supply comes from snowmelt from the drainage area around the lake, and occasional runoff

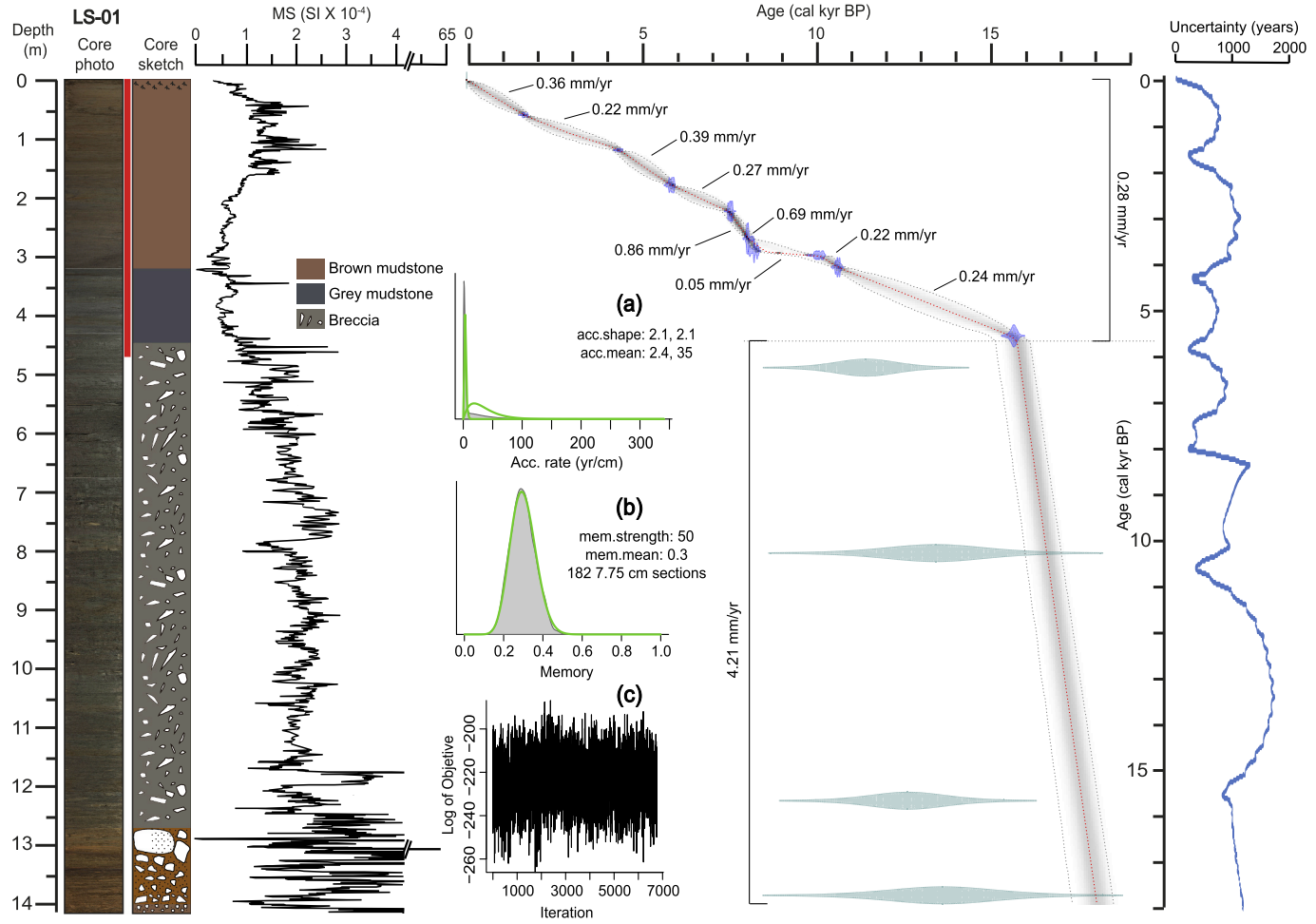


**Fig. 2.** LS-01 core lithology, magnetic susceptibility (MS in SI units x $10^{-4}$) and bayesian age model (with estimated sedimentary rates in mm/yr). The section of the core studied here of the topmost 4.7 m is shown in red in the lithological plot. On the right is a plot with down-core uncertainty ranges plotted on age. For more details about the lithology and age model see López-Avilés et al. (2022). (For interpretation of the references to colour in this figure legend, the reader is referred to the web version of this article.)

events. The LS basin bedrock is composed of low-degree metamorphic mica schists of the Nevado Filábride complex (Martín Martín et al., 2010).

The climate in the study area is typically Mediterranean, with mild winters and hot and dry summers. Climatic data for LS are not directly available, but a weather station located ~3.5 km from the study site at 2200 m elevation shows a mean annual precipitation of 581 mm and a mean annual temperature of 6.3 ± 0.5 °C. The driest month is July with 2 mm and the most humid month is March with 114 mm of rainfall. February is the coldest month (−1.2 ± 1.7 °C) and July the warmest one (16.8 ± 1.2 °C) (Organismo Autónomo Parques Nacionales, 2021).

The present-day vegetation in the Sierra Nevada is largely controlled by temperature and precipitation/humidity gradients and thus depends on the elevation (Valle, 2003; Fig. 1G). Above ~2800 m asl, climate is characterized by very cold winters, short growing season, high solar radiation and snowfall, and strong winds. In this context, soils are meager and a tundra-like shrubby grassland develops. This cryoromediterranean vegetation belt is characterized by species of Poaceae, Asteraceae, Brassicaceae and Plantaginaceae between other herbs, including several endemic plants (*Erigeron frigidus*, *Saxifraga nevadensis* and *Viola crassiuscula*) (Valle, 2003). The underlying oromediterranean vegetation belt is located between ~1900–2800 m asl, and is mostly characterized by conifers, such as *Pinus sylvestris*, *P. nigra*, *Juniperus hemisphaerica*, *J. sabina* and *J. communis* subsp. *nana*, as well as woody species of Fabaceae, Cistaceae and Brassicaceae. The supramediterranean belt, between ~1400–1900 m asl, is characterized by *Quercus pyrenaica*, *Q. faginea*, *Q. rotundifolia*, *Acer opalus* subsp. *granatense* and *Fraxinus angustifolia* among other trees/shrubs and some herbs such as *Artemisia glutinosa*. The mesomediterranean vegetation belt, between ~600–1400 m asl, is mainly dominated by *Quercus rotundifolia* with a characteristic *Retama sphaerocarpa* understorey (Valle, 2003). *Quercus coccifera* and *Pistacia lenticus* are the main taxa in the lowest elevation thermomediterranean vegetation belt (~0–600 m asl). LS is located at the upper elevational limit of the oromediterranean vegetation belt and treeline in the study area, located at ~2300 m asl, mostly composed of *P. sylvestris* (Fig. 1D). However, the study area has been modified by high anthropogenic activity and was reforested with *P. sylvestris* in the mid-20th century (Arias Abellán, 1981). Therefore, it is difficult to place the natural elevation of treeline in Sierra Nevada, which seems to have been artificially lowered down several hundred meters (Lorite et al., 2022).

## 3. Materials and methods

The 14.1 m-long LS-01 sedimentary record was recovered from the depocenter of the LS basin in September 2014 using a Rolatec RL-48-L coring machine from the Scientific Instrumentation Center of the University of Granada (CIC-UGR) (Fig. 1). The cores were transported to the UGR, stored in a refrigerated room at 4 °C and eventually were split and imaged in the laboratory at UGR and CIC, respectively. Lithologic description and sedimentological analysis were previously carried out by López-Avilés et al. (2022) (Fig. 2). To develop an age model for the LS-01 sediment core, we used radiocarbon analyses from the topmost organic-rich part of the record and OSL analyses for the detrital-rich

**Table 1**
Age data for LS-01. Radiometric ages were calibrated using IntCal20.14c curve (Reimer et al., 2020) with Calib 8.2 (http://calib.org/calib/). OSL dates are marked with asterisk. In red colour are the radiocarbon dates not used in the age model. Acronyms: TBS; pre-treated bulk sediment with HCl and HF, BS; bulk sediment.

| Laboratory code | Material | Depth (m) | Dating method | Age $^{14}$C yr BP ± 1σ OSL* | Calibrated age (cal yr BP) 2σ range |
|---|---|---|---|---|---|
| Reference Age | | 0 | Present | | -65 |
| Beta-544146 | TBS | 0.37 | $^{14}$C | 11070 ± 30 | 12910 - 13088 |
| Beta-452041 | TBS | 0.60 | $^{14}$C | 1690 ± 30 | 1528 - 1695 |
| Beta-544147 | TBS | 0.83 | $^{14}$C | 15960 ± 40 | 19129 - 19425 |
| Beta-452042 | TBS | 1.20 | $^{14}$C | 3880 ± 30 | 4160 - 4414 |
| Beta-452043 | TBS | 1.80 | $^{14}$C | 5050 ± 30 | 5720 - 5903 |
| Beta-458581 | TBS | 2.26 | $^{14}$C | 6620 ± 40 | 7431 - 7570 |
| Beta-458581 | TBS | 2.72 | $^{14}$C | 7200 ± 30 | 7939 - 8158 |
| Beta-458583 | TBS | 2.94 | $^{14}$C | 7380 ± 30 | 8037 - 8324 |
| Poz-72963 | Algae | 3.00 | $^{14}$C | 8920 ± 50 | 9821 - 10219 |
| Poz-72964 | TBS | 3.00 | $^{14}$C | 11580 ± 60 | 13317 - 13580 |
| Beta-458584 | TBS | 3.21 | $^{14}$C | 9370 ± 30 | 10505 - 10686 |
| Poz-72965 | BS | 3.60 | $^{14}$C | 30900 ± 400 | 34541 - 36090 |
| Beta-544148 | TBS | 3.81 | $^{14}$C | 23860 ± 100 | 27748 - 28288 |
| Beta-544149 | TBS | 4.38 | $^{14}$C | 13050 ± 40 | 15474 - 15795 |
| OSL-LS-Dr.09 | | 4.83 - 5.02 | OSL | 11400 ± 800* | |
| Poz-72966 | BS | 5.40 | $^{14}$C | 37200 ± 800 | 40679 - 42578 |
| OSL-LS-Dr.14 | | 8.03 - 8.17 | OSL | 13400 ± 1300* | |
| Poz-72967 | BS | 9.00 | $^{14}$C | 33800 ± 600 | 36956 - 40089 |
| OSL-LS-Dr.21 | | 12.29 - 12.39 | OSL | 12600 ± 1000* | |
| OSL-LS-Dr.24 | | 13.89 - 14.01 | OSL | 13600 ± 1400* | |

bottom (López-Avilés et al., 2022; Fig. 2). Previous analyses on the LS-01 core included magnetic susceptibility (MS), total organic carbon and C/N (López-Avilés et al., 2022; Fig. 2).

The topmost ~4.7 m part of the LS-01 sedimentary record, characterized by fine-grained sediments, was sampled for palynological analysis every 5 cm. This section of the core contains a sedimentary record of the last ~15.8 kyr based on the age model described in López-Avilés et al. (2022) (Table 1; Fig. 2). A total of 94 samples of two cubic centimeters were collected. The pollen extraction method followed a modified Faegri and Iversen (1989) method. One tablet with a known number of *Lycopodium* spores for calculation of pollen concentration was added to the samples. Sediment samples were processed with HCl (35%) and HF (45%) to remove the carbonates and silicates, respectively, from the sediment and concentrate the organic matter. The samples were sieved at 10 μm to remove particles smaller than the pollen grains. The residual material, together with glycerin, was mounted on microscope slides. Counting, and identification, of palynomorphs was carried out with a Leica DM1000 LED transmitted light microscope at 400× magnifications. Pollen atlases, such as Beug (1961) and pollen reference material of plants that occur in southern Spain were used for certain identifications. *Pinus* pollen was divided into two categories: *Pinus* indeterminate and *P. sylvestris* type (most-likely including *P. sylvestris* and/or *P. nigra*). *P. sylvestris* type pollen was differentiated from the rest of *Pinus* indeterminate pollen by its small size (generally with a total grain size smaller than 85 μm) (Desprat et al., 2015). Pollen percentages in each analyzed sample have been calculated with respect to the total sum of terrestrial pollen. The most representative pollen types with occurrences higher than 1% are shown in Fig. 3. The percentages of non-pollen palynomorphs (NPP), including algae such as *Botryococcus, Pediastrum, Debarya, Spirogyra* and *Zygnema*, dinoflagellate cysts (dinocysts), *Isoetes* microspores, oocytes of the aquatic flatworm *Neorhabdocoela,* mycorrhizal chlamydospores of *Glomus* and spores of the liverwort *Riccia* have been calculated with respect to the total sum of terrestrial pollen plus NPP and are shown in Fig. 4. The pollen climate index (PCI), used in previous studies to discriminate between cold/arid and warm/humid climates (e.g., Joannin et al., 2011; Camuera et al., 2019, 2021), and calculated with the ratio of mesothermic (*Quercus*, *Olea*, *Betula* and *Corylus*) / steppic taxa (*Artemisia*, *Lygeum*, *Ephedra* and Amaranthaceae), was also calculated here (Fig. 5). Cluster analyses of the pollen and NPP data were performed using the program CONISS (Grimm, 1987), with the aim of grouping samples with similar pollen assemblages into pollen zones (Figs. 3 and 4).

Charcoal particles bigger than 30 μm were counted in the palynological slides. Charcoal concentration (charcoal particles/cm$^3$) was calculated using the *Lycopodium* tracer concentration (Figs. 3 and 5) in this way: #charcoal particles/#*Lycopodium* tracers *9666 (being 9666 the number of *Lycopodium* tracers in 1 tablet).

## 4. Results

The LS-01 pollen record is made up of 42 samples that provided sufficient pollen for statistical analyses. Fifty-two samples were barren in pollen. The pollen record is generally characterized by the relevance of the forest component, which is dominated by *Pinus* species, most likely including *P. sylvestris* (that grows in the area at present) or *P. nigra.* To a lesser extent, the pollen spectra show evergreen and deciduous *Quercus, Juniperus, Olea, Betula* and *Corylus*. Regarding the herbaceous and shrubby taxa, pollen assemblages are dominated by Poaceae, *Artemisia*, Asteraceae Asteroideae, Asteraceae Cichorioideae, Amaranthaceae, Caryophyllaceae, *Plantago*, and in smaller proportions, Ericaceae, *Ephedra, Lygeum,* Rosaceae, Onagraceae, Geraniaceae and Cistaceae. Cyperaceae and Ranunculaceae are also relatively abundant and represent the aquatic plants (Fig. 3). With respect to the NPP, *Pediastrum*, *Botryococcus, Spirogyra, Zygnema* and *Debarya*, are abundant. *Isoetes, Riccia*, *Glomus*, *Neorhabdocoela* and dinocysts also occur (Fig. 4). Charcoal concentration varies considerably through time (Fig. 3).

The pollen and NPP frequencies fluctuate considerably through time and can be subdivided into several environmental and climatically distinct periods (zones) that roughly agree with the subdivision of the latest Pleistocene (HS1, B-A and YD; Rasmussen et al., 2006) and Holocene Series/Epoch (Early, Middle and Late Holocene; Walker et al., 2018; Figs. 3 and 4). Below, we describe the LS pollen and NPP data for each of the identified zones.

### 4.1. Pollen and NPP zone 1 (between ~ 15.8–14.2 kyr; 470–405 cm depth)

This palynological zone might roughly corresponds in timing with the HS1 and B-A transition. *P. sylvestris / nigra,* shows maxima during this zone with percentages averaging ~95%. Asteraceae Asteroideae, *Artemisia* and Amaranthaceae increased slightly at the end of this zone (Fig. 3). Charcoal shows relatively low concentrations. The aquatic alga *Pediastrum* is most abundant in this zone presenting two peaks. The alga *Botryococcus* peaks during the *Pediastrum* minimum. Zygnemataceae zygospores (*Debarya*, *Spirogyra* and *Zygnema)* are abundant. *Neorhabdocoela* occurs with maximum frequencies in this zone (Fig. 4).

### 4.2. Pollen and NPP zone 2 (between ~ 14.2–12.7 kyr; 405–370 cm depth)

This palynological zone approximately corresponds to the B-A (Figs. 3 and 4). *Pinus* decreases considerably, initially reaching ~40%.

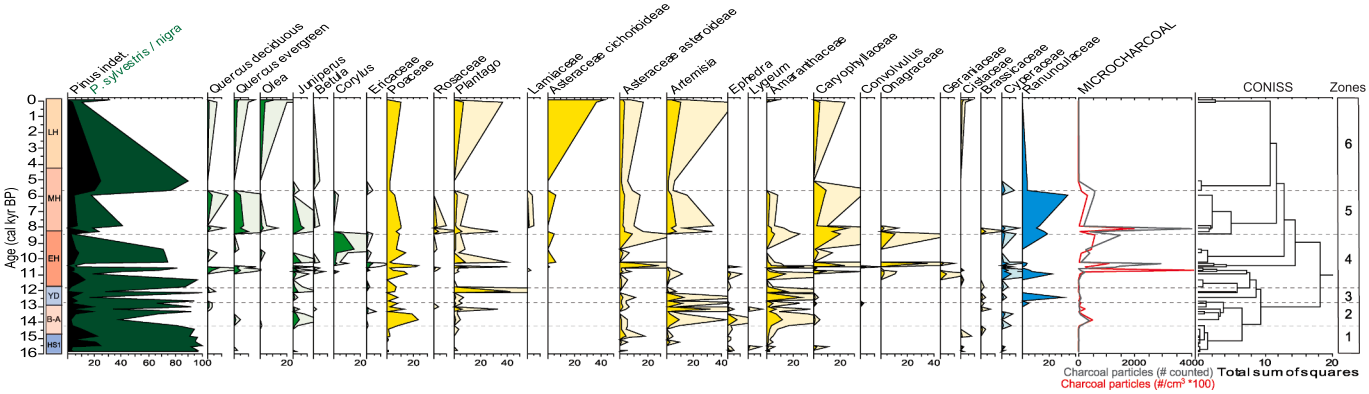


**Fig. 3.** Detailed pollen and charcoal diagram from the LS-01 core showing percentages of selected taxa (higher than 1%). In green, yellow and blue are the trees, herbs and wetland angiosperm taxa, respectively. The pollen zonation on the right was made using cluster analysis provided by CONISS (Grimm, 1987). Light shadings indicate a 5× exaggeration scale. HS1, B-A, YD, EH, MH and LH stand for Heinrich Stadial-1, Bolling-Allerod, Younger Dryas, Early Holocene, Middle Holocene and Late Holocene. (For interpretation of the references to colour in this figure legend, the reader is referred to the web version of this article.)

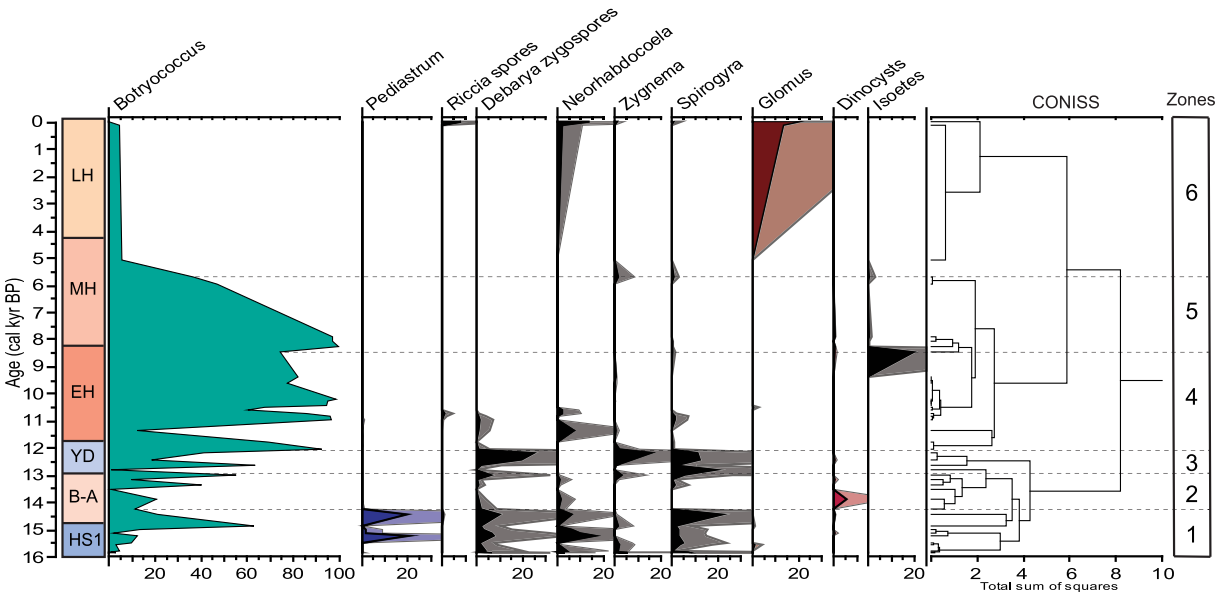


**Fig. 4.** Detailed non-pollen palynomorph (NPP) diagram from the LS-01 core. The NPP zonation on the right was made using cluster analysis provided by CONISS (Grimm, 1987). Light shadings indicate a 5× exaggeration scale. HS1, B-A, YD, EH, MH and LH stand for Heinrich Stadial-1, Bolling-Allerod, Younger Dryas, Early Holocene, Middle Holocene and Late Holocene.

Subsequently, it shows two oscillations, with peaks ~90% and a minimum of ~40%. *Juniperus* increased at the beginning of this zone. Herbaceous taxa such as Poaceae, *Artemisia*, *Ephedra* and Amaranthaceae increase. *Artemisia* shows maximum values at the end of this zone. Charcoal shows higher abundance. *Pediastrum* and *Botryococcus*, together with the Zygnemataceae and *Neorhabdocoela*, decrease considerably, whereas dinocysts show maximum values.

### *4.3. Pollen and NPP zone 3 (between ~ 12.7–11.8 kyr; 370–350 cm depth)*

This zone is correlated with the YD (Figs. 3 and 4). *Pinus* shows marked variability, with two maxima and two minima with values between 95 and 20%. Herbs such as *Artemisia, Plantago* and Amaranthaceae peak in this zone, with the latest showing maximum values. The aquatic Ranunculaceae increase, showing a peak at this time. Charcoal particles decrease and show minimum values. With respect to the NPP, the microalgae *Botryococcus* and Zygnemataceae (including *Debarya*, *Spirogyra* and *Zygnema*), increase. *Neorhabdocoela* is absent while the dinocysts decline.

### *4.4. Pollen and NPP zone 4 (between ~ 11.8–8.4 kyr; 350–290 cm depth)*

This zone approximately corresponds to the EH (Figs. 3 and 4). *Pinus* is fluctuating with a decreasing trend, reaching two minima of ~5% at 10.5 and 8.4 kyr. *Juniperus* and both evergreen and deciduous *Quercus* increase in this zone. Deciduous *Quercus* shows the record's maximum at ~10.6 kyr. Ericaceae, *Betula and Corylus* also increase, with the latter showing an increasing trend and maximum values at the end of the EH. Herbs such as Poaceae, Caryophyllaceae, Onagraceae and Geraniaceae increase, whereas *Artemisia* decrease, showing minimum values of the record between ~10.5–8.4 kyr. The aquatic Cyperaceae show maximum occurrences during the EH, peaking together with Ranunculaceae at ~11 kyr. Charcoal concentration increase considerably, showing maxima between 11 and 10.2 and 9.4–8.4 kyr. *Botryococcus* increase significantly during the EH whereas other algae such as Zygnemataceae (including *Debarya*, *Spirogyra* and *Zygnema*) decrease. *Neorhabdocoela* only occur at the beginning of this zone and *Isoetes* occurs with a peak at the end of the EH.

### *4.5. Pollen and NPP zone 5 (between ~ 8.4–5.6 kyr; 290–170 cm depth)*

This zone corresponds to most of the MH (Figs. 3 and 4) and is characterized by the minimum values of *Pinus,* averaging 20%. Other forest species such as evergreen and deciduous *Quercus*, *Juniperus* and *Olea* are relatively abundant during this period. With respect to the herbs, *Artemisia* and Caryophyllaceae increase in this zone. The aquatic Ranunculaceae shows maximum values of the record whereas Cyperaceae decrease. Charcoal concentration is characterized by a peak at the beginning of the MH at ~8.0 kyr but declines during the rest of the MH. The NPP are mostly represented by *Botryococcus*, which shows maximum occurrences between 8.4 and 7.8 kyr, decreasing considerably during the rest of the MH.

### *4.6. Pollen and NPP zone 6 (between ~ 5.6 kyr-present; 170–0 cm depth)*

This palynological zone corresponds to the latest MH and Late Holocene (LH; Figs. 3 and 4). It is characterized by the increase in *Pinus*, depicting a peak at ~5 kyr, and a subsequent decrease until present. In general, other forest species show very low occurrences during this zone, except for the last centuries, when several increases in *Pinus*, *Olea* and *Quercus* are observed. The herbaceous component including *Artemisia*, Asteraceae Cichorioideae, Poaceae, *Plantago*, Caryophyllaceae and Cistaceae, show increases during this period. The aquatics and charcoal concentration decrease considerably during the LH. With respect to the algae, *Botryococcus* decrease significantly. Other NPP such as *Neorhabdocoela* or *Glomus* increase in the last centuries.

## 5. Discussion

Pollen analyses from the Sierra Nevada have been previously reported as proxies for regional vegetation and climate changes (Anderson et al., 2011; Jiménez-Moreno and Anderson, 2012; Ramos-Román et al., 2016, 2018a, 2018b; Mesa-Fernández et al., 2018; Camuera et al., 2019, 2021). Increases in subalpine and temperate Mediterranean forest species in the alpine records, summarized here by the PCI (Figs. 5 and 6), point to increases in humidity and temperature. Trees need relatively high soil water supply, while mountain forest taxa move to higher elevation during climate warmings (Lenoir et al., 2008; Gottfried et al.,

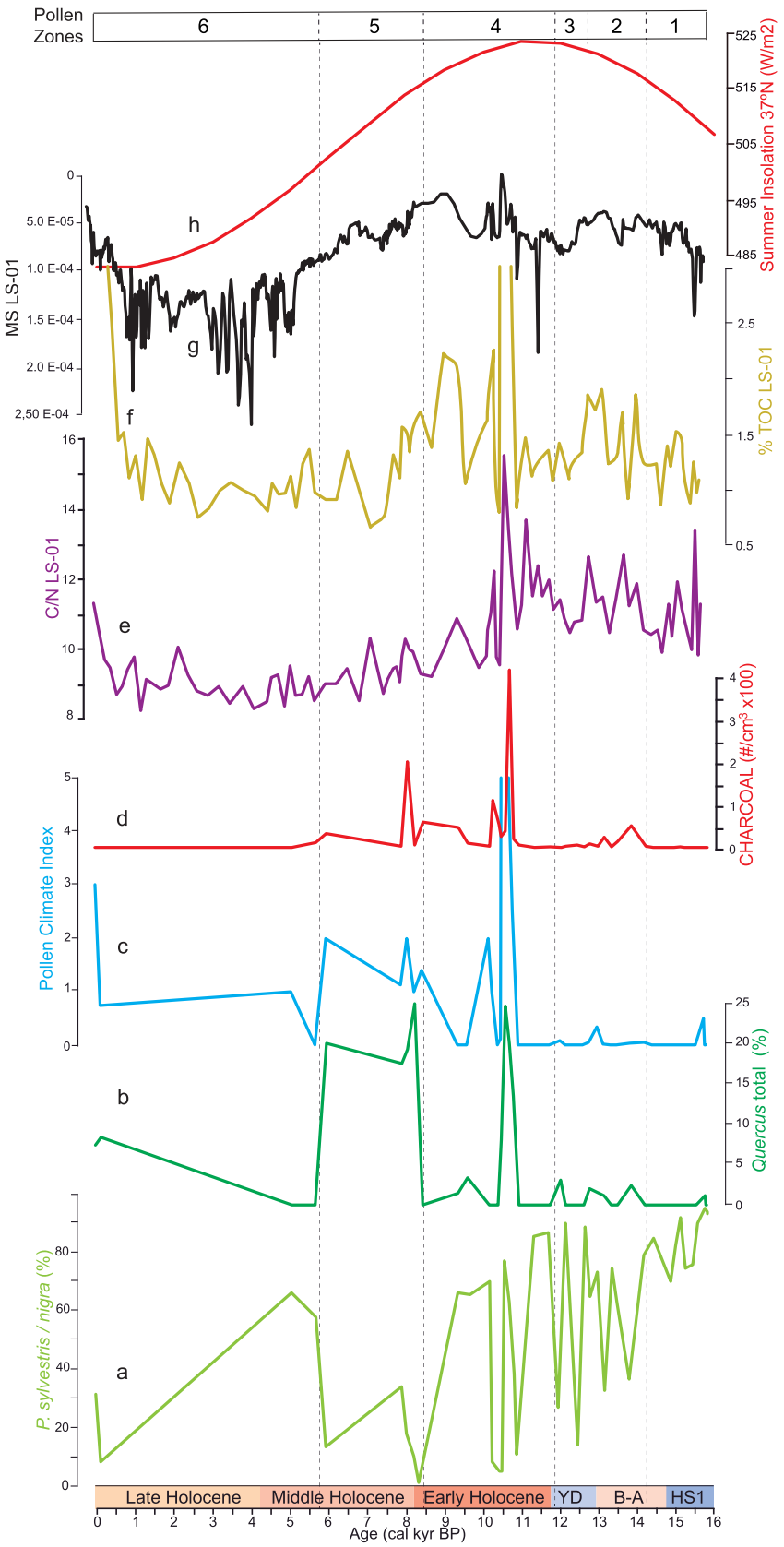


**Fig. 5.** Comparison of paleoenvironmental and paleoclimatic proxies from the LS-01 core. (A) *P. sylvestris* type pollen abundance. (B) *Quercus* total pollen in percentages. (C) Pollen Climate Index (PCI; see text for explanation). (D) Microcharcoal concentration. (E) C/N ratios from López-Avilés et al. (2022). (F) Total Organic Carbon (TOC) from López-Avilés et al. (2022). (G) Magnetic susceptibility (MS; SI x $10^{-4}$) from López-Avilés et al. (2022). Note the scale is inverted. (H) Summer insolation for 37°N (Laskar et al., 2004). Pollen zones are shown at the top (see Fig. 3). HS1, B-A, YD, EH, MH and LH stand for Heinrich Stadial-1, Bølling-Allerød, Younger Dryas, Early Holocene, Middle Holocene and Late Holocene.

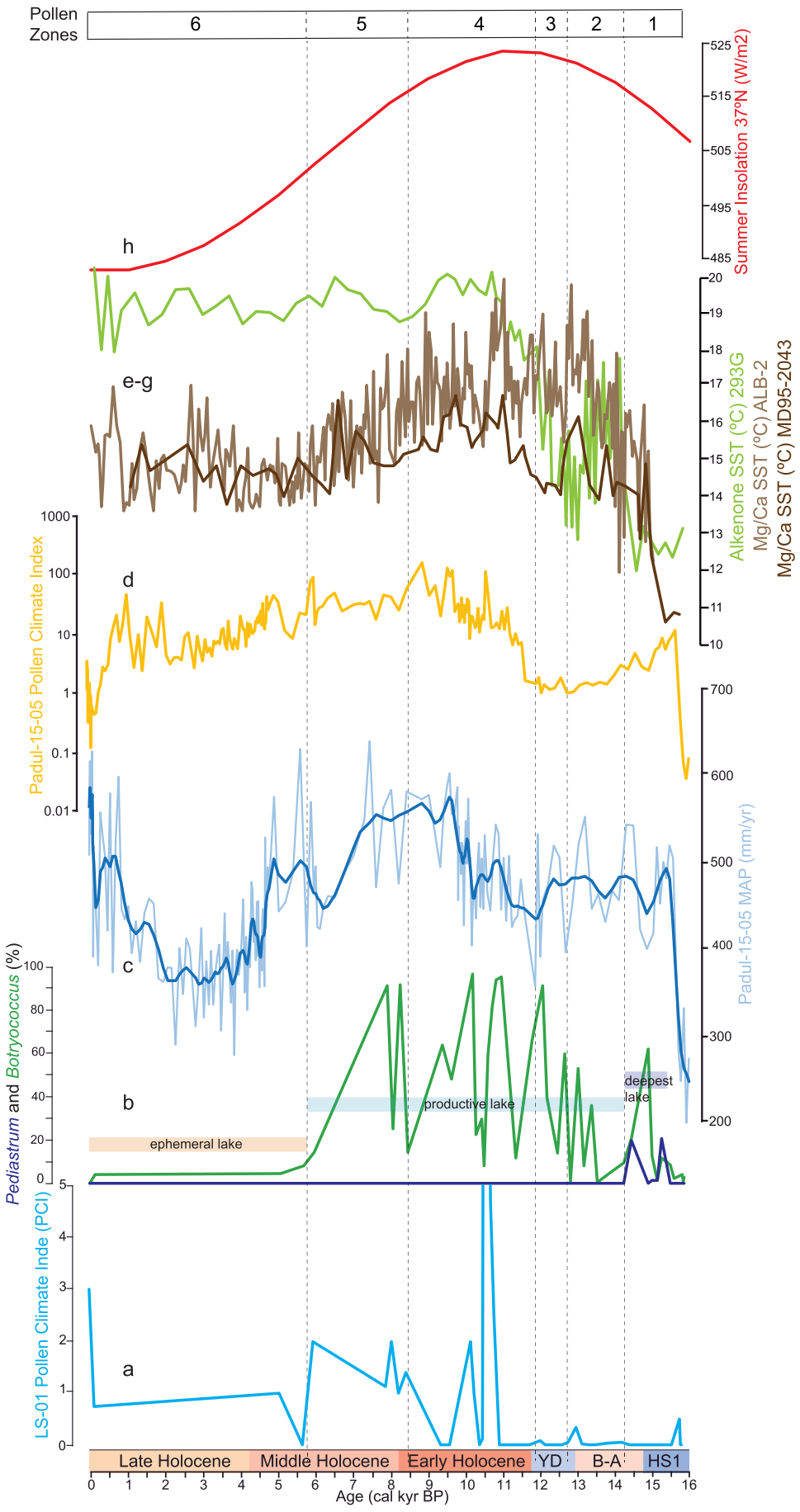


(caption on next page)

**Fig. 6.** Comparison of paleoenvironmental and paleoclimatic proxies from the LS-01 core with other paleoclimatic records from the southern Iberian Peninsula and summer insolation for the last 16 kyr. (A) Pollen Climate Index (PCI; see text for explanation) from the LS-01 core. (B) *Pediastrum* and *Botryococcus* algae abundances from LS-01 core and indications about lake level and productivity. (C) Mean Annual Precipitation (MAP) estimated from the Padul-15-05 pollen record (Camuera et al., 2022). (D) Pollen Climate Index (PCI) from the Padul-15-05 pollen record (Camuera et al., 2019). (*E*-G) Sea Surface Temperature (SST) reconstructed from *G. bulloides* Mg/Ca ratios from marine core ALB-2 (Alboran Sea; Català et al., 2019), SST (°C) reconstructed from *G. bulloides* Mg/Ca ratios from marine core MD95–2043 (Català et al., 2019) and SST (°C) reconstructed from alkenones from marine sediment core 293G (Rodrigo-Gámiz et al., 2014). (H) Summer (August) insolation values at 37°N (Laskar et al., 2004). Pollen zones are shown at the top (see Fig. 3). HS1, B-A, YD, EH, MH and LH stand for Heinrich Stadial-1, Bølling-Allerød, Younger Dryas, Early Holocene, Middle Holocene and Late Holocene.

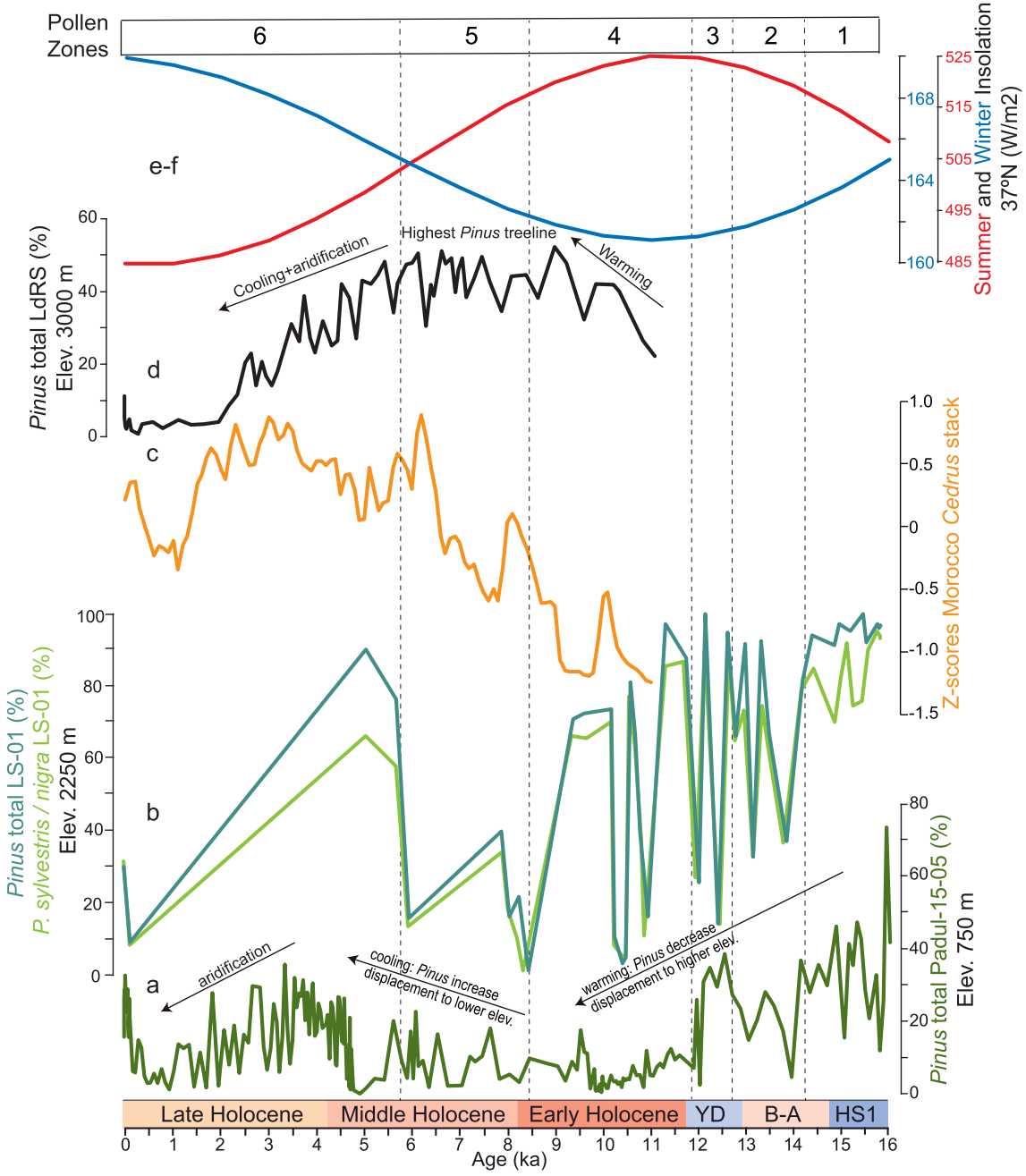


**Fig. 7.** Comparison of *Pinus* pollen records from the Sierra Nevada with *Cedrus* synthetic record from Morocco for the last 16 kyr. (A) *Pinus* total pollen from Padul-15-05 core (Ramos-Román et al., 2018a, 2018b; Camuera et al., 2019). (B) *Pinus* total and *P. sylvestris* type pollen abundances from LS-01 core. (C) Synthetic Morocco z-scores Holocene *Cedrus* stack (Jiménez-Moreno et al., 2020). (D) *Pinus* total pollen from Laguna de Río Seco, Sierra Nevada (Anderson et al., 2011). (E-F) Summer (red line) and winter (blue line) insolation values at 37°N (Laskar et al., 2004). Pollen zones are shown at the top (see Fig. 3). HS1, B-A, YD, EH, MH and LH stand for Heinrich Stadial-1, Bølling-Allerød, Younger Dryas, Early Holocene, Middle Holocene and Late Holocene. (For interpretation of the references to colour in this figure legend, the reader is referred to the web version of this article.)

2012; Jiménez-Moreno et al., 2022). In Sierra Nevada, the most frequent high-altitude forest species are pines such as *P. sylvestris* and *P. nigra.* (i.e., the oromediterranean vegetation belt, between ~1900–2800 m). Fluctuations in their frequencies during the latest Pleistocene and Holocene sediments might reflect displacements in elevation due to shifts in climate (see for example Anderson et al., 2011; Jiménez-Moreno and Anderson, 2012; Fig. 7).

Lake levels from Sierra Nevada also responded to past climate changes, predominantly conditioned by variations in the precipitation-evaporation balance, with higher lake levels during cold and/or humid periods and lower lake levels during warm and/or arid periods (Anderson et al., 2011; Camuera et al., 2018, 2019; López-Avilés et al., 2022). Planctonic microalgae (*Pediastrum*, *Botryococcus*, *Debarya, Spirogyra*, *Zygnema*), wetland angiosperms (Cyperaceae, Ranunculaceae), and other organisms (such as the aquatic flatworm *Neorhabdocoela*), are conditioned by lake levels and shore surface area. The relative abundance of these taxa changed through the different climatically distinct periods (zones), providing us with information about lake depth, nutrients and productivity. Here below we show that the surrounding vegetation and organisms inhabiting the LS environment responded very sensitively to climate changes that occurred in the last ~16 kyr in the western Mediterranean area.

### 5.1. Late Pleistocene and Holocene vegetation and climate reconstruction

#### 5.1.1. HS1 and B-A transition (~15.8–14.2 kyr)

The low PCI values of the LS pollen record show cold and dry conditions during the end of HS1 and early B-A (Figs. 5 and 6). This is conditioned by the highest percentage of cryophilous *Pinus* in the LS pollen record, which is most-likely explained because this alpine area was barren of vegetation during deglaciation and the *Pinus* pollen depositing in LS originates from long-distance transport from lower elevations (see section below). It is well-known that *Pinus* pollen is usually overrepresented in pollen records because pine trees produce large quantities of pollen and bisaccate pollen (i.e., pollen with air sacs) gets transported very well and for long distances by wind (Heusser, 1988). Cold climate conditions in LS agree with previous regional studies showing that HS1 was one of the coldest and driest periods of the last glaciation, indicated by the lowest PCI values from Padul (Camuera et al., 2019, 2021) and sea surface temperature (SST) records from Alboran Sea (Rodrigo-Gámiz et al., 2014; Català et al., 2019) (Fig. 6).

The LS NPP record shows that the deepest lake conditions of the last ~16 kyr occurred during the HS1-B-A transition between ~15.5–14.2 kyr (Fig. 3). This is supported by *Pediastrum* maxima (Fig. 6), which is a colonial alga previously interpreted as an indicator of oligotrophic to mesotrophic deepwater lake conditions (Nielsen and Sørensen, 1992; Kaufman et al., 2010; Anderson et al., 2020). The abundance of other algae such as *Botryococcus, Debarya*, *Spirogyra* and *Zygnema* also peaked at that climate transition, further supporting deep lake conditions. Increasing but still low summer insolation probably enhanced ice melting and the glacier retreat in the Sierra Nevada, generating runoff and the formation of a deep lake in LS. Cold conditions also favored little evaporation in the LS area during summer, which further controlled the precipitation/evaporation balance increasing lake levels in the area, such as observed in Padul (Camuera et al., 2018, 2019). The deepest lake conditions in LS starting at ~15.7 kyr were also previously interpreted by the sedimentological analysis of the LS sedimentary sequence characterized by organic-rich clays (i.e., grey mudstone; Fig. 2; López-Avilés et al., 2022). Variability in the algal abundance is observed at the HS1-B-A transition with *Botryococcus* peaking during a minimum of *Pediastrum* at ~14.8 kyr. This could represent a lowering of the lake level and increase in productivity at this time, as *Botryoccocus*, also a colonial green microalga, has previously been suggested as indicator of shallow and eutrophic waters (Batten and Grenfell, 1996; Guy-Ohlson, 1992; Jiménez-Moreno et al., 2007). The occurrence of *Neorhabdocoela* flatworm eggs during this period indicates that the maximum LS lake levels must have been established within the photic zone (commonly in lakes, the first 10 m; Haas, 1996). This is inferred from *Neorhabdocoela*, which feeds on rotifers and diatoms and produces oocytes - thick-walled resting-eggs - for propagation and for survival under drought-induced stress (Haas, 1996).

Minima in charcoal concentration during HS1 (Figs. 3 and 5) indicates very low fire activity at this time probably related to pine forest openness and cold climate conditions. Low forest fuel due to cold-dry climate conditions would have occurred at that time (Camuera et al., 2019). Present-day natural fires are infrequent above the treeline and they were possibly quite rare in the past. Therefore, we postulate that charcoal particles originated from lower altitudes, where pines were most abundant during the last glacial (Camuera et al., 2019), and were transported by wind to higher elevations in the Sierra Nevada.

#### 5.1.2. Bølling-Allerød (B-A; ~14.2–12.7 kyr)

Climate warming occurred in southern Spain, including the Sierra Nevada, and the western Mediterranean area during the B-A (García-Alix et al., 2014; Rodrigo-Gámiz et al., 2014; Català et al., 2019; Camuera et al., 2019, 2021; Fig. 6) and glaciers receded and most-likely disappeared from the alpine area (Palacios et al., 2016). Xerophytic herbs such as *Artemisia*, *Ephedra*, and several species of Amaranthaceae, Poaceae, together with *Juniperus*, colonized the area and reached maxima during the late B-A, probably indicating their expansion in the barren areas left by glaciers after deglaciation and *Pinus* pollen decreased (Fig. 3). Mesic forest expansion due to warmer and more humid conditions occurred at lower elevations in the Sierra Nevada (Camuera et al., 2019, 2021; Fig. 6) but its pollen signal does not seem to reach the studied alpine environment. Unlike the widely distributed *Pinus*, pollen of these mesic elements is not widely dispersed.

Lake levels most-likely decreased during the B-A due to increasing summer insolation, generating warming and more evaporative conditions. This is indicated by the decrease in *Pediastrum* and *Botryococcus*, together with the Zygnemataceae and *Neorhabdocoela*. On the other hand, dinocysts show maximum values during this period, perhaps indicating specific lake water conditions that are unknown.

Charcoal increased timidly during B-A (Figs. 3 and 5), probably indicating long-distance transport from the increase in fire activity at lower elevation due to the enhanced forest (fuel) caused by warmer conditions (Camuera et al., 2019; Daniau et al., 2007).

#### 5.1.3. Younger Dryas (YD; ~12.7–11.8 kyr)

Colder and drier conditions with respect to the B-A occurred in the western Mediterranean area during the YD (Rodrigo-Gámiz et al., 2014; Català et al., 2019; Camuera et al., 2019; Fig. 6). This is indicated in the LS record by maxima of xerophytes such as Amaranthaceae, *Plantago* (most-likely the cold-adapted *P. nivalis*) and *Artemisia,* together with an increase in cryophilous *Pinus* pollen, coming from lower elevations. Colder climate conditions agree with a previous interpretation of the sedimentary record from LS that shows frost-shattered breccias deposited within the lacustrine facies in another core close to the eastern shore (LS-03), and a decrease in TOC and an increase in MS in LS-01 (Fig. 5) linked to enhanced periglacial activity (López-Avilés et al., 2022).

LS lake levels increased during the Younger Dryas, probably due to a decrease in evaporation. This is shown in the LS record by the overall increase in algae such as *Botryococcus* and Zygnemataceae (including *Debarya*, *Spirogyra* and *Zygnema*), which in turn indicate very productive conditions (indicated by the increase in *Botryococcus*). However, lake levels never reached the maximum levels of HS1, as *Pediastrum* is absent. The aquatic Ranunculaceae must have been benefited from this rise in lake level, perhaps due to the increase in the shore surface area where they occur.

Charcoal particles decreased and show minimum values at this time, pointing to a decrease in fire activity in the Sierra Nevada lowlands caused by the decrease in temperature and increase in openness of the forest (Camuera et al., 2019).

*5.1.4. Early Holocene (EH) warm and humid period (~11.8–8.4 kyr)*

The LS pollen record shows that maxima in temperature and humidity of the last ~16 kyr occurred during the EH. This is shown by the abundance of temperate and mesophytes such as deciduous *Quercus, Betula, Corylus* and Ericaceae and maxima in aquatic plants such as Cyperaceae. Xerophytes show minima of the record at this time. These vegetation dynamics are reflected in the PCI pollen ratio, depicting maximum values between 10.6 and 10.0 kyr (Figs. 5 and 6). The increase in temperate and mesophilous forest species is interpreted as a response to warmer and more humid climate, producing a displacement of tree species towards higher altitudes and more dense forests. A sedimentological study from LS also interpreted warmest and wettest conditions of the Holocene occurring at ~10.6 kyr, shown by the highest values of organic matter (TOC), with a contributed mixture of terrestrial vascular plants and aquatic algae (C/N), and the lowest detrital content of the sedimentary record (MS) (López-Avilés et al., 2022; Fig. 5). This study agrees with other palynological records from the alpine Sierra Nevada area that indicate maxima in temperature and humidity conditions between ~10.5 and 7.0 kyr, indicated by the highest abundance of forest species, indicating the highest elevation of treeline, and the abundance of algae (*Botryococcus* and *Pediastrum*) (Anderson et al., 2011; Jiménez-Moreno and Anderson, 2012; Ramos-Román et al., 2018a, 2018b; Mesa-Fernández et al., 2018; Camuera et al., 2019; Fig. 6). In the lower elevation Padul-15-05 record, the highest values of Mediterranean forest also occurred at that time, showing an expansion in mesic forest species (Ramos-Román et al., 2018b). Organic geochemistry paleoclimatic proxy records from the Sierra Nevada area agree with this and other previous works also depicting warmest (Rodrigo-Gámiz et al., 2022) and wettest (Toney et al., 2020; García-Alix et al., 2021) conditions during the EH. Other western Mediterranean regional studies show warmest conditions during the EH and earliest MH (Fletcher and Sánchez-Goñi, 2008; Rodrigo-Gámiz et al., 2014; Català et al., 2019; Gomes et al., 2020; Fig. 6). Warmest conditions during the EH can be explained by orbitally-forced summer insolation maxima (Laskar et al., 2004; Figs. 5 and 6). The maximum humidity between ~10.5 and 7.0 kyr could be explained by an increase in the land/sea temperature contrast in the Mediterranean region during the fall season, which would have favored an increase in rainfall during fall and winter seasons (Meijer and Tuenter, 2007).

The NPP record from LS shows that *Botryococcus* increased during the EH, while the rest of the algae almost vanished, which could indicate that the lake became progressively shallower and became more and more productive during the EH until 8.2 kyr, when a peak in *Botryococcus* occurred (Fig. 6).

Fire activity shows a similar pattern to the temperate and mesophilous forest represented by the PCI, showing maxima between 11.0 and 10.2 and 9.4–8.4 kyr, during the warmest and most humid period detected in the area (Fig. 5). This fire pattern might be related to the close relationship between fire activity and fuel loads on the landscape in this Mediterranean area, as previously observed in other paleoecological records (Daniau et al., 2007; Linstädter and Zielhofer, 2010; Jiménez-Moreno et al., 2013; Ramos-Román et al., 2016).

*5.1.5. Middle Holocene (MH) transitional climate (~8.4–5.6 kyr)*

The Early and Middle Holocene transition occurred here at ~8.4 kyr is characterized by an environmental and climate change towards somewhat drier and colder climate conditions. This is indicated in the LS record by the decrease in temperate and mesophilous forest pollen taxa including *Betula* or *Corylus* and the increase in xerophytes such as *Artemisia* and Caryophyllaceae, which is reflected in PCI values lower than during the EH. The LS record agrees with other pollen records from.

Sierra Nevada and the southern Iberian Peninsula that show a progressive forest decrease and an increase in xerophytes, pointing to a climate aridification and cooling that began around 7.0 kyr and intensified after ~6.0–5.0 kyr (Carrión, 2002; Fletcher et al., 2010; Jiménez-Moreno et al., 2015; Ramos-Román et al., 2018a; Mesa-Fernández et al., 2018; Gomes et al., 2020; Jiménez-Moreno et al., 2022). Cooling in the MH is also shown by SST records from the Alboran Sea (Rodrigo-Gámiz et al., 2014; Català et al., 2019) and can be explained by the decline in summer insolation (Cacho et al., 2002; Renssen et al., 2003) (Fig. 6).

The NPP record from LS shows that the lake level lowered during the MH. This is pointed out by the algal record from LS, mostly represented by *Botryococcus*, which exhibits a decreasing trend after depicting maximum values at the EH-MH transition at ~8.2 kyr between 8.4 and 7.8 kyr (Figs. 4 and 6). A lowering of the LS lake levels was previously interpreted with the sedimentological properties of the LS sediments, with a lowering of the organic matter (productivity) and increase in detritic content (López-Avilés et al., 2022; Fig. 5). A considerable decline in aquatic algae species indicating decreasing lake levels due to aridification during the MH and LH has also been observed in other records from the alpine Sierra Nevada (Anderson et al., 2011; Jiménez-Moreno and Anderson, 2012).

Charcoal concentration is characterized by a peak at the beginning of the MH at ~8.0 kyr but decreases during the rest of the MH (Figs. 3 and 5). The charcoal peak at ~8.0 kyr coincides with a maximum in *Quercus* total (and PCI) that could further support the fuel-fire relationship previously observed (Fig. 5). Decreasing forest species in the MH due to the climate aridification trend most-likely translated into fewer forest fires in the Sierra Nevada area.

*5.1.6. Late Holocene (LH; ~5.6 kyr-present)*

With the limitations of the low resolution of the pollen record for this period, the LS record shows that the aridification and cooling process enhanced during the last 5.6 kyr. This is indicated by the decrease in *Quercus* species, *Juniperus*, and aquatics such as Ranunculaceae, and the increase in xerophytes such as *Artemisia* and Asteraceae Cichorioideae, which are reflected in the PCI decrease (Figs. 5 and 6). The long-term aridification trend observed in the western Mediterranean region from the Middle Holocene to the present (Jiménez-Moreno and Anderson, 2012; Jiménez-Espejo et al., 2014; Ramos-Román et al., 2016, 2018a; Mesa-Fernández et al., 2018; García-Alix et al., 2021, 2022) triggered the evolution from permanent to ephemeral lacustrine conditions with an increase in aquatic productivity in the LS basin that ended up in the LH with the current summer desiccation of the lake. The NPP record from LS shows minima in the abundance of algae (mostly *Botryococcus*) during the LH, probably indicating seasonal lake conditions during the LH until present (Fig. 6). A seasonal lake most likely triggered the oxidation and decomposition of pollen in many intervals of the LH, which explains the low pollen resolution for that time period.

*Olea*, *Pinus* and *Quercus* (and thus PCI) increased in the last centuries (Figs. 3 and 5) indicating anthropogenic activities such as olive cultivation at lower altitudes, especially intensive in the last millennium (Ramos-Román et al., 2019), and reforestation with pines and oaks in the last century (see synthesis in Jiménez-Moreno et al., 2022). A greater soil erosion and contribution of allochthonous detrital materials is observed in the last centuries, interpreted from the increase in *Glomus* endomycorrhizal fungus in the LS sediment samples (Fig. 4). The abundance of *Glomus* in paleoecological records has been related to enhanced rates of soil erosion and other mechanical soil disturbances (Anderson et al., 1984; Van Geel et al., 1989), which could also be related to recent human impact in the LS area. The previous sedimentological study of the LS sedimentary sequence shows a significant increase in organic content and a change in the C/N in the last ~500 years that was interpreted as an anthropically-forced seasonal lake eutrophication and/or soil erosion in the catchment area (López-Avilés et al., 2022). The peak in *Riccia* during the last centuries (Fig. 4) may well indicate enhanced grazing pressure in the Sierra Nevada, as this liverwort presently grows associated with grazing areas in emergent surfaces of mountain water bodies (Carrión, 2002).

Microcharcoal analysis from the LS record shows very little fire activity in the LH, agreeing with the diminishing trend in vegetation and

fuel (Fig. 5). However, previous studies in the Sierra Nevada show enhanced forest fires in the last ~3.0 kyr, especially during the Iberian Roman Humid Period and between 3.1 and 1.6 kyr, coinciding in time with relatively wet period of the LH (Jiménez-Moreno et al., 2013; Ramos-Román et al., 2016). Besides a climate control, anthropogenically enhanced fire activity in the last 3.0 kyr should also be considered. In this sense it seems that human influence in LH fire regimes in the Iberian Peninsula may have been complex, with agricultural expansion both promoting and suppressing fire occurrence (Shen et al., 2022).

### 5.2. Pine forest dynamics since deglaciation in mountain areas of the southern Iberian Peninsula

The LS and other pollen records show that pine forests were an important component of the last glacial vegetation in the southern Iberian Peninsula (this study; Fernández et al., 2007; Carrión et al., 2010, 2019; Desprat et al., 2015; Camuera et al., 2019; Ochando et al., 2020). Pines were the most predominant trees in an open woodland landscape located at low elevations in the southern Iberian Peninsula (González-Sampériz et al., 2010; Rubiales et al., 2010; Camuera et al., 2019), as during the Last Glaciation, alpine, subalpine and oromediterranean pine species (mostly *P. nigra* and *P. sylvestris*) were displaced to the *meso* and thermomediterranean vegetation belts (Badal et al., 2008; Carrión et al., 2010; Camuera et al., 2019). Small occurrences of *Quercus*, and the sporadic presence of other thermophilous species such as *Olea* or *Pinus pinaster,* indicate that glacial refugia for temperate taxa may have existed in protected coastal shelves and valleys located at low elevation in the area (Carrión, 2002; González-Sampériz et al., 2010; Camuera et al., 2019).

The *Pinus* pollen species identifications in the LS, Laguna de la Mosca, Padul and other pollen records from southern Iberian Peninsula such as Siles Lake or the marine site MD95–2042, show that the most occurring pine species were high-elevation cryophilous pines such as *P. nigra* and *P. sylvestris* (this study; Carrión, 2002; Desprat et al., 2015; Manzano et al., 2019; Camuera et al., 2019). This is confirmed by macrofossil findings of *P. nigra* in last glacial sediments from southern Spain (Postigo-Mijarra et al., 2010).

Previously published pollen studies from sites located at different elevations in the Sierra Nevada range show significant differences in the dynamics of the *Pinus* pollen abundance during the Holocene (Fig. 7). These are mostly explained by the different site elevation and their relative distance to the supramediterranean cryophilous *Pinus* forest vegetation belt that moved upslope or downslope through time, mostly depending on the temperature evolution since deglaciation (e.g., Camuera et al., 2019). For example, the Laguna de Río Seco, Laguna de la Mosca and Borreguiles de la Virgen alpine pollen records, located above treeline at ~2900–3000 m and about 30 km west of LS (see location in Fig. 1), show a pattern very similar to the summer insolation, showing that treeline and *Pinus* forest displaced towards higher elevations (closer to the studied sites) during the EH, stabilized during the early MH and displaced towards lower elevations (farther away from the alpine study sites) during the late MH and LH (Anderson et al., 2011; Jiménez-Moreno and Anderson, 2012; Manzano et al., 2019). The lower elevation Padul-15-05 pollen record at ~700 m shows the opposite *Pinus* pollen percentage evolution, showing an overall decreasing trend during the EH, stabilization during the late EH and early MH and an increase-decrease pattern in the late MH and LH. The *Pinus* pollen record from LS, despite its relatively high elevation at 2259 m and the generally higher relative abundances, depicts a pattern more similar to the lower elevation Padul site than the other Sierra Nevada alpine lakes (Fig. 7). In fact, similar percentages of *Pinus* are reached during HS1 in the LS and Padul records, which can be explained because the LS area was barren of vegetation during deglaciation and the *Pinus* pollen reaching LS originates from long-distance transport from lower elevations. Cryophilous *Pinus* and lower vegetation belts (with for example *Quercus* species) started moving to higher elevations during the B-A, and *Pinus* shows a decrease in the Padul record but also in the LS record, probably indicating that long-distance *Pinus* pollen transport was still important at that time. An interruption of the climate warming occurred during the YD, producing a relative increase in the *Pinus* pollen in the Padul and the airborne *Pinus* pollen-influenced LS record. *Pinus* continued moving towards higher elevations due to climate warming during the EH, which is reflected in the *Pinus* peak in the earliest Holocene from LS and the increasing values in the alpine pollen records (Fig. 7). *Pinus* forest reached the highest treeline in the Sierra Nevada in the EH and early MH between ~9.5 and 7.0 kyr (Fig. 7). It seems like the supramediterranean vegetation belt with *Pinus* occurred above LS, as *Pinus* decreased in LS but showed maxima in the higher elevation sites. The late MH and LH in the high-elevation records from Sierra Nevada are characterized by a general decreasing trend in *Pinus* due to the displacement of supramediterranean vegetation belt towards lower elevations mostly caused by the decrease in summer insolation lowering temperatures and precipitation. However, an increasing and decreasing trends in *Pinus* are observed in the LS and lower elevation sites during the late MH and LH. The increasing trend could be explained by the lowering of the *Pinus* vegetation belt towards lower elevations closer to LS and Padul due to climate cooling (Fig. 7). In addition, the decrease in summer insolation would trigger lower summer evaporation in the study area, benefiting the growth of cool-adapted montane tree species such as *Pinus* in southern Spain or *Cedrus* in northern Africa (equivalent in ecological requirements to the cryophilous pines in the Sierra Nevada; Fig. 7; Jiménez-Moreno et al., 2020). The decrease in precipitation and the enhanced aridification process previously described in many paleoclimatic records from Sierra Nevada and the southern Iberian Peninsula during the Late Holocene most-likely forced the decrease in *Pinus* and in general of forest species on the mountain areas (see the decrease in *Pinus* in both high and low elevations in Fig. 7) until *Pinus* reforestation in the last ~100 years (see section above).

## 6. Conclusions

The palynological analysis, together with a multiproxy analysis, of a sedimentary record from Laguna Seca, permitted us to reconstruct the vegetation and the environmental change mostly due to climate variations during the last ~16 kyr in the Sierra Nevada, southern Spain. Vegetation and lake environments in Sierra Nevada were very sensitive to climate change related with orbital-scale insolation dynamics but also to millennial-scale climate variability since the last deglaciation. The comparison of the paleoenvironmental and paleoclimate results from this study with other records from the Sierra Nevada and the southern Iberian Peninsula allowed us to conclude:

1. This palynological record shows cold and dry climatic conditions and the deepest lake levels in LS during the HS1-B-A transition.
2. Climate warming occurred in southern Spain, including the Sierra Nevada, and the western Mediterranean area during the B-A due to increasing summer insolation, diminishing the LS lake levels.
3. Colder and drier conditions occurred in the western Mediterranean area during the YD. LS lake levels increased, probably due to a decrease in evaporation.
4. The LS pollen record shows that maxima in temperature and humidity of the last ~16 kyr occurred during the EH. The LS lake became progressively shallower and became progressively more productive during the EH until 8.2 kyr.
5. A climate shift towards drier and colder climate conditions occurred at the Early and Middle Holocene transition, provoking vegetation changes and lowering of lake levels during the MH.
6. An aridification and cooling process enhanced during the last 5.6 kyr, which triggered the evolution from permanent to ephemeral lacustrine conditions in LS.

7. The study shows that fire activity in the LS area during the last ~16 kyr was mostly related with the abundance of forest fuel on the landscape in this Mediterranean area.
8. Anthropogenic impact through cultivation, reforestation, cattle grazing, enhanced erosion and eutrophication, is evident in the last centuries.
9. This study highlights the importance of cryophilous pines such as *P. nigra* and *P. sylvestris* in the vegetation evolution of mountain areas in the southern Iberian Peninsula related with climate change.

## Declaration of Competing Interest

The authors declare that they have no known competing financial interests or personal relationships that could have appeared to influence the work reported in this paper.

## Data availability

Data will be made available on request.

## Acknowledgements

This study was supported by the I + D + i projects CGL2013-47038-R, CGL2017-85415-R, PID2019-1049449GB-I00, and PID2021-125619OB-C21/C22 funded by Ministerio Ciencia e Innovación/Agencia Estatal de Investigación/ 10.13039/501100011033/ and Fondo Europeo de Desarrollo Regional "Una manera de hacer Europa", I + D + i projects A-RNM-336-UGR20 and P20_00059 of the action "Proyectos I + D + i del Programa Operativo FEDER - Junta de Andalucía - UGR" and the research group RNM-190. This research is part of the project "Thematic Center on Mountain Ecosystem & Remote sensing, Deep learning-AI e-Services University of Granada-Sierra Nevada" (LifeWatch-2019-10-UGR-01), which has been co-funded by the Ministry of Science and Innovation through the FEDER funds from the Spanish Pluriregional Operational Program 2014-2020 (POPE), LifeWatch-ERIC action line. José Carrión was supported by the I + D + I project PID2019-1049449 GB-I00 funded by MCIN/AEI/ 10.13039/501100011033/ and FEDER "Una manera de hacer Europa" and the fellowship 20788/PI/18 of Fundación Séneca. We thank Javier Jaimez for his help with the core drilling in Laguna Seca and Alejandro Navarro and Aurora Baquera for the sediment sampling. ALA acknowledges the predoctoral fellowship BES- 2018-084293 provide by the MCIN/ AEI/ 10.13039/501100011033/. CLB acknowledges the European Union for her Marie Sklodowska-Curie grant agreement number 892487 under Horizon 2020 funds. JC acknowledges the Ministerio de Ciencia e Innovación of the Spanish Government for the grant number FJC2020-044215-I of the Juan de la Cierva Formación postdoctoral program.

## References

Alba-Sánchez, F., Abel-Schaad, D., López-Saez, J.A., Sabariego-Ruiz, S., Pérez-Díaz, S., Luelmo-Lautenschlaeger, R., Garrido-García, J.A., 2021. Early anthropogenic change in western Mediterranean mountains (Sierra Nevada, SE Spain). Anthropocene 33, 100278.

Ali, E., Cramer, W., Carnicer, J., Georgopoulou, E., Hilmi, N.J.M., Cozannet, G.Le, Lionello, P., 2022. Cross-Chapter Paper 4: Mediterranean Region. In: Pörtner, H.-O., Roberts, D.C., Tignor, M., Poloczanska, E.S., Mintenbeck, K., Alegría, A., Craig, M., Langsdorf, S., Löschke, S., Möller, V., Okem, A., Rama, B. (Eds.), Climate Change 2022: Impacts, Adaptation and Vulnerability. Contribution of Working Group II to the Sixth Assessment Report of the Intergovernmental Panel on Climate Change. Cambridge University Press, Cambridge, UK and New York, NY, USA.

Anderson, R.S., Homola, R.L., Davis, R.B., Jacobson Jr., G.L., 1984. Fossil remains of the mycorrhizal fungal Glomus fasciculatum complex in postglacial lake sediments from Maine. Can. J. Bot. 62, 2325–2328.

Anderson, R.S., Jimenez-Moreno, G., Belanger, M., Briles, C., 2020. Fire history of the unique high-elevation Snowmastodon (Ziegler Reservoir) site during MIS 6-4, with comparisons of TII to TI in the southern Colorado Rockies. Quat. Sci. Rev. 232, 106213.

Anderson, R.S., Jiménez-Moreno, G., Carrión, J.S., Pérez-Martínez, C., 2011. Holocene vegetation history from Laguna de Río Seco, Sierra Nevada, southern Spain. Quat. Sci. Rev. 30, 1615–1629.

Arias Abellán, J.A., 1981. In: La repoblación forestal en la vertiente norte de Sierra Nevada. Cuadernos geográficos de la Universidad de Granada, pp. 283–305.

Arroyo, J., Abellán, P., Arista, M., Ariza, M.J., de Castro, A., Escudero, M., Lorite, J., Martínez-Borda, E., Mejías, J.A., Molina-Venegas, R., Pleguezuelos, J.M., Simón-Porcar, V., Viruel, J., 2022. Sierra Nevada, a Mediterranean biodiversity super hotspot. In: Zamora, R., Oliva, M. (Eds.), The Landscape of the Sierra Nevada. Springer Nature Switzerland AG, pp. 11–31.

Badal, E., Bonet, H., Collado, E., Fabado, J., Fuentes, M., Izquierdo, I., Mata, C., Moreno, A., Ntinou, M., Quixal, D., Ripollès, P.P., Soria, L., 2008. Lo real y lo imaginario. El proyecto Hum2004-04939 sobre la flora en el mundo Ibérico. In: Rovira, S., García-Heras, M., Gener, M., Montero, I. (Eds.), Actas VII Congreso Ibérico de Arqueometría, Madrid, pp. 144–157.

Batten, D.J., Grenfell, H.R., 1996. Botryococcus. In: Jansonius, J., McGregor, D.C. (Eds.), Palynology: Principles and Applications, vol. 1. American Association of Stratigraphic Palynologists Foundation, pp. 205–214.

Beug, H.J., 1961. Leitfaden der Pollenbestimmung, 1. Fischer, Stuttgart, p. 63.

Cacho, I., Grimalt, J.O., Canals, M., 2002. Response of the Western Mediterranean Sea to rapid climatic variability during the last 50,000 years: a molecular biomarker approach. J. Mar. Sys. 33–34, 253–272.

Camuera, J., Jiménez-Moreno, G., Ramos-Román, M.J., García-Alix, A., Toney, J.L., Anderson, R.S., Jiménez-Espejo, F.J., Kaufman, D., Bright, J., Webster, C., Yanes, Y., Carrión, J.S., Ohkouchi, N., Suga, H., Yamame, M., Yokoyama, Y., Martínez-Ruiz, F., 2018. Orbital-scale environmental and climatic changes recorded in a new ~ 200,000-year-long multiproxy sedimentary record from Padul, southern Iberian Peninsula. Quat. Sci. Rev. 198, 91–114.

Camuera, J., Jiménez-Moreno, G., Ramos-Román, M.J., García-Alix, A., Toney, J.L., Anderson, R.S., Jiménez-Espejo, F., Bright, J., Webster, C., Yanes, Y., Carrión, J.S., 2019. Vegetation and climate changes during the last two glacial-interglacial cycles in the western Mediterranean: a new long pollen record from Padul (southern Iberian Peninsula). Quat. Sci. Rev. 205, 86–105.

Camuera, J., Jiménez-Moreno, G., Ramos-Román, M.J., García-Alix, A., Jiménez-Espejo, F.J., Toney, J.L., Anderson, R.S., 2021. Chronological control and centennial-scale climatic subdivisions of the last Glacial termination in the western Mediterranean region. Quat. Sci. Rev. 255, 106814.

Camuera, J., Ramos-Román, M.J., Jiménez-Moreno, G., García-Alix, A., Ilvonen, L., Ruha, L., Gil-Romera, G., González-Sampériz, P., Seppä, H., 2022. Past 200 kyr hydroclimate variability in the western Mediterranean and its connection to the African Humid periods. Sci. Rep. 12, 9050.

Carrión, J.S., 2002. Patterns and processes of late Quaternary environmental change in a montane region of southwestern Europe. Quat. Sci. Rev. 21, 2047–2066.

Carrión, J.S., Fernández, S., González-Sampériz, P., Gil-Romera, G., Badal, E., Carrión-Marco, Y., López-Merino, L., López-Sáez, J.A., Fierro, E., Burjachs, F., 2010. Expected trends and surprises in the Lateglacial and Holocene vegetation history of the Iberian Peninsula and Balearic Islands. Rev. Palaeobot. Palynol. 162, 458–475.

Carrión, J.S., Fernández, S., Jiménez, J., Munuera Giner, M., Ochando, J., Amorós, G., Ponce de León, M., Zollikofer, Ch., Martín-Lerma, I., Toro-Moyano, I., Hajdas, I., Walker, M.J., 2019. The sequence at Carihuela Cave and its potential for research into Neanderthal ecology and the Mousterian in southern Spain. Quat. Sci. Rev. 217, 194–216.

Català, A., Cacho, I., Frigola, J., Pena, L.D., Lirer, F., 2019. Holocene hydrography evolution in the Alboran Sea: a multi-record and multiproxy comparison. Clim. Past 15, 927–942.

Daniau, A.L., Sánchez-Goñi, M.F., Beaufort, L., Laggoun-Défarge, F., Loutre, M.F., Duprat, J., 2007. Dansgaard-Oeschger climatic variability revealed by fire emissions in southwestern Iberia. Quat. Sci. Rev. 26, 1369–1383.

Desprat, S., Díaz Fernández, P.M., Coulon, T., Ezzat, L., Pessarossi-Langlois, J., Gil, L., Morales-Molino, C., Sánchez Goñi, M.F., 2015. Pinus nigra (European black pine) as the dominant species of the last glacial pinewoods in south-western to Central Iberia: a morphological study of modern and fossil pollen. J. Biogeogr. 42 (10), 1998–2009.

Faegri, K., Iversen, J., 1989. Textbook of Pollen Analysis. Wiley, New York.

Fernández, S., Carrión, J.S., Fuentes, N., González-Sampériz, P., Montoya, E., Gil-Romera, G., Vega-Toscano, L.G., Riquelme, J.A., 2007. Palynology of Carihuela Cave, southern Spain: completing the record. Geobios 40, 75–90.

Fletcher, W.J., Sánchez-Goñi, M.F., 2008. Orbital and sub-orbital scale climate impacts on the vegetation of the W. Mediterranean basin during the last 48 000 years. Quat. Res. 70, 451–464.

Fletcher, W.J., Sánchez-Goñi, M.F., Peyron, O., Dormoy, I., 2010. Abrupt climate changes of the last glaciation detected in a Western Mediterranean forest record. Clim. Past 6, 245–264.

García-Alix, A., Jiménez-Moreno, G., Anderson, R.S., Jiménez-Espejo, F., Delgado-Huertas, A., 2012. Holocene paleoenvironmental evolution of a high-elevation wetland in Sierra Nevada, southern Spain, deduced from an isotopic record. J. Paleolimnol. 48, 471–484.

García-Alix, A., Jimenez-Espejo, F.J., Lozano, J.A., Jiménez-Moreno, G., Martínez-Ruiz, F., García Sanjuán, L., Aranda Jiménez, G., García Alfonso, E., Ruiz-Puertas, G., Anderson, R.S., 2013. Anthropogenic impact and lead pollution throughout the Holocene in southern Iberia. Sci. Total Environ. 449, 451–460.

García-Alix, A., Jiménez-Espejo, F.J., Toney, J.L., Jiménez-Moreno, G., Ramos-Román, M.J., Anderson, R.S., Ruano, P., Queralt, I., Delgado Huertas, A., Kuroda, J., 2017. Alpine bogs of southern Spain show human-induced environmental change superimposed on long-term natural variations. Sci. Rep. 7, 7439.

García-Alix, A., Jiménez-Espejo, F.J., Jiménez-Moreno, G., Toney, J.L., Ramos-Román, M.J., Camuera, J., Anderson, R.S., Delgado Huertas, A., Martínez-Ruiz, Queralt, I., 2018. Holocene geochemical footprint from Semi-arid alpine wetlands in southern Spain. Sci. Data 5, 180024.

García-Alix, A., Jiménez-Moreno, G., Jiménez-Espejo, F.J., García-García, F., Delgado Huertas, A., 2014. An environmental snapshot of the Bølling interstadial in Southern Iberia. Quat. Res. 81, 284–294.
García-Alix, A., Toney, J.L., Jiménez-Moreno, G., Pérez-Martínez, C., Jiménez, L., Rodrigo-Gámiz, M., Anderson, R.S., Camuera, J., Jiménez-Espejo, F.J., Peña-Angulo, D., Ramos-Román, M.J., 2020. Algal lipids reveal unprecedent warming rates in alpine areas of SW Europe during the Industrial Period. Clim. Past 16, 245–263.
García-Alix, A., Camuera, J., Ramos-Román, M.J., Toney, J.L., Sachse, D., Schefuß, E., Jiménez-Moreno, G., Jiménez-Espejo, F.J., López-Avilés, A., Anderson, R.S., Yanes, Y., 2021. Paleohydrological dynamics in the Western Mediterranean during the last glacial cycle. Glob. Planet. Chang. 202, 103527.
García-Alix, A., Jiménez-Moreno, G., Gázquez, F., Monedero-Contreras, R., López-Avilés, A., Jiménez-Espejo, F.J., Rodríguez-Rodríguez, M., Camuera, J., Ramos-Román, M.J., Anderson, R.S., 2022. Climatic control on the Holocene hydrology of a playa-lake system in the western Mediterranean. Catena 214, 106292.
Gomes, S.D., Fletcher, W.J., Rodrigues, T., Stone, A., Abrantes, F., Naughton, F., 2020. Time-transgressive Holocene maximum of temperate and Mediterranean forest development across the Iberian Peninsula reflects orbital forcing. Palaeogeogr. Palaeoclimatol. Palaeoecol. 550, 109739.
González-Sampériz, P., Leroy, S.A.G., Carrión, J.S., Fernández, S., García-Antón, M., Gil-García, M.J., Uzquiano, P., Valero-Garcés, B., Figueiral, I., 2010. Steppes, savannahs, forests and phytodiversity reservoirs during the Pleistocene in the Iberian Peninsula. Rev. Palaeobot. Palynol. 162, 427–457.
Gottfried, M., Pauli, H., Futschik, A., Akhalkatsi, M., Barancok, P., Benito Alonso, J.L., Coldea, G., Dick, J., Erschbamer, B., Fernández Calzado, M.A.R., et al., 2012. Nat. Clim. Chang. 2, 111–115.
Grimm, E.C., 1987. CONISS: a Fortran 77 program for stratigraphically constrained cluster analysis by the method of incremental sum of squares. Comput. Geosci. 13, 13–35.
Guy-Ohlson, D., 1992. Botryococcus as an aid of the interpretation of palaeoenvironment and depositional processes. Palaeogeogr. Palaeoclimatol. Palaeoecol. 71, 1–15.
Haas, J.N., 1996. Neorhabdocoela oocytes – palaeoecological indicators found in pollen preparations from the Holocene freshwater lake sediments. Rev. Palaeobot. Palynol. 91, 371–382.
Heusser, L.E., 1988. Pollen distribution in marine sediments on the continental margin of Northern California. Mar. Geol. 80, 131–147.
Jiménez-Espejo, F.J., García-Alix, A., Jiménez-Moreno, G., Martínez-Ruiz, F., Anderson, R.S., Rodríguez-Tovar, F.J., Giralt, S., Rodrigo-Gámiz, M., Delgado-Huertas, A., Pardo-Igúzquiza, E., 2014. Saharan aeolian input and effective humidity variations over Western Europe during the Holocene. Chem. Geol. 374–375, 1–12.
Jiménez-Moreno, G., Abdul Aziz, H., Rodríguez-Tovar, F.J., Pardo-Igúzquiza, E., Suc, J.-P., 2007. Palynological evidence for astronomical forcing in Early Miocene lacustrine deposits from Rubielos de Mora Basin (NE Spain). Palaeogeogr., Palaeoclimatol., Palaeoecol. 252, 601–616.
Jiménez-Moreno, G., Anderson, R.S., 2012. Holocene vegetation and climate change recorded in alpine bog sediments from the Borreguiles de la Virgen, Sierra Nevada, southern Spain. Quat. Res. 77, 44–53.
Jiménez-Moreno, G., García-Alix, A., Hernández-Corbalán, M.D., Anderson, R.S., Delgado-Huertas, A., 2013. Vegetation, fire, climate and human disturbance history in the southwestern Mediterranean area during the late Holocene. Quat. Res. 79, 110–122.
Jiménez-Moreno, G., Rodríguez-Ramírez, A., Pérez-Asensio, J.N., Carrión, J.S., López-Sáez, J.A., Villarías-Robles, J.J., Celestino-Pérez, S., Cerrillo-Cuenca, E., León, A., 2015. Impact of late-Holocene aridification trend, climate variability and geodynamic control on the environment from a coastal area in SW Spain. The Holocene 25, 607–617.
Jiménez-Moreno, G., Anderson, R.S., Ramos-Román, M.J., Camuera, J., Mesa-Fernández, J.M., García-Alix, A., Jiménez-Espejo, F.J., Carrión, J.S., López-Avilés, A., 2020. The Holocene Cedrus pollen record from Sierra Nevada (S Spain), a proxy for climate change in N Africa. Quat. Sci. Rev. 242, 106468.
Jiménez-Moreno, G., García-Alix, A., Anderson, R.S., Ramos-Román, M.J., Camuera, J., Mesa-Fernández, J.M., Toney, J.L., Jiménez-Espejo, F.J., Carrión, J.S., López-Avilés, A., Rodrigo-Gámiz, M., Webster, C.E., 2022. Reconstruction of past environment and climate using wetland sediment records from the Sierra Nevada. In: Zamora, R., Oliva, M. (Eds.), The Landscape of the Sierra Nevada. Springer Nature Switzerland AG, pp. 95–114.
Joannin, S., Bassinot, F., Combourieu Nebout, N., Peyron, O., Beaudouin, C., 2011. Vegetation response to obliquity and precession forcing during the Mid-Pleistocene transition in Western Mediterranean region (ODP site 976). Quat. Sci. Rev. 30, 280–297.
Kaufman, D., Anderson, R.S., Hu, F.S., Berg, E., Werner, A., 2010. Evidence for a variable and wet Younger Dryas in southern Alaska. Quat. Sci. Rev. 29, 1445–1452.
Laskar, J., Robutel, P., Joutel, F., Gastineau, M., Correia, A.C.M., Levrard, B., 2004. A long-term numerical solution for the insolation quantities of the Earth. Astron. Astrophys. 428, 261–285.
Lenoir, J., Gégout, J.C., Marquet, P.A., de Ruffray, P., Brisse, H.A., 2008. Significant upward shift in plant species optimum elevation during the 20th Century. Science 320, 1768–1771.
Linstädter, A., Zielhofer, C., 2010. Regional fire history shows abrupt responses of Mediterranean ecosystems to centennial-scale climate change (Olea-Pistacia woodlands), NE Morocco. J. Arid Environ. 74, 101–110.
López-Avilés, A., García-Alix, A., Jiménez-Moreno, G., Anderson, R.S., Toney, J.L., Mesa-Fernández, J.M., Jiménez-Espejo, F.J., 2021. Latest Holocene paleoenvironmental and paleoclimate reconstruction from an alpine bog in the Western Mediterranean region: the Borreguil de los Lavaderos de la Reina record (Sierra Nevada). Palaeogeogr. Palaeoclimatol. Palaeoecol. 573, 110434.
López-Avilés, A., Jiménez-Moreno, G., García-Alix, A., García-García, F., Camuera, J., Anderson, R.S., Sanjurjo-Sánchez, J., Chamorro, C.A., Carrión, J.S., 2022. Post-glacial evolution of alpine environments in the western Mediterranean region: the Laguna Seca record. Catena 211, 106033.
Lorite, J., Lamprecht, A., Peñas, J., Rondinel-Mendoza, K., Fernandez-Calzado, R., Benito, B., Cañadas, E., 2022. Altitudinal patterns and changes in the composition of high mountain plant communities. In: Zamora, R., Oliva, M. (Eds.), The landscape of the Sierra Nevada. Springer Nature Switzerland AG, pp. 171–193.
Manzano, S., Carrión, J.S., López-Merino, L., et al., 2019. A palaeoecological approach to understanding the past and present of Sierra Nevada, a southwestern european biodiversity hotspot. Glob. Planet. Chang. 175, 238–250.
Martín Martín, J.M., Braga Alarcón, J.C., Gómez Pugnaire, M.T., 2010. Geological Routes of Sierra Nevada. Regional Ministry for the Environment, Junta de Andalucía.
Meijer, P.Th., Tuenter, E., 2007. The effect of precession-induced changes in the Mediterranean freshwater budget on circulation at shallow and intermediate depth. J. Mar. Sys. 68, 349–365.
Mesa-Fernández, J.M., Jiménez-Moreno, G., Rodrigo-Gámiz, M., García-Alix, A., Jiménez-Espejo, F.J., Martínez-Ruiz, F., Anderson, R.S., Camuera, J., Ramos-Román, M.J., 2018. Vegetation and geochemical response to Holocene rapid climate change in the Sierra Nevada (southeastern Iberia): the Laguna Hondera record. Clim. Past 14, 1687–1706.
Nielsen, H., Sørensen, I., 1992. Taxonomy and stratigraphy of late-glacial Pediastrum taxa from Lysmosen, Denmark e a preliminary study. Rev. Palaeobot. Palynol. 74, 55–75.
Ochando, J., Carrión, J.S., Rodríguez-Vidal, J., Jiménez-Arenas, J.M., Fernández, S., Amorós, G., Munuera, M., Scott, L., Stewart, J.R., Knull, M.V., Toro-Moyano, I., Ponce de León, M., Zollikofer, C., 2020. Palynology and chronology of hyaena coprolites from the Piñar karstic caves Las Ventanas and Carihuela, southern Spain. Palaeogeogr. Palaeoclimatol. Palaeoecol. 552, 109771.
Nacionales, Organismo Autónomo Parques, 2021. https://www.miteco.gob.es/es/red-parques-nacionales/red-seguimiento/acceso-datos.aspx (accessed 20 June 2021).
Palacios, D., Gómez-Ortiz, A., Andrés, N., Salvador, F., Oliva, M., 2016. Timing and new geomorphologic evidence of the Last Deglaciation stages in Sierra Nevada (southern Spain). Quat. Sci. Rev. 150, 10–129.
Páscoa, P., Gouveia, C.M., Russo, A., Trigo, R.M., 2017. Drought trends in the Iberian Peninsula over the last 112 years. Adv. Meteorol. 2017, 4653126.
Postigo-Mijarra, J.M., Gómez Manzaneque, F., Morla Juaristi, C., Zazo, C., 2010. Palaeoecological significance of Late Pleistocene pine macrofossils in the lower Guadalquivir Basin (Doñana natural park, southwestern Spain). Palaeogeogr. Palaeoclimatol. Palaeoecol. 295, 332–343.
Ramos-Román, M.J., Jiménez-Moreno, G., Anderson, R.S., 2016. Centennial-scale vegetation and North Atlantic Oscillation changes during the late Holocene in the western Mediterranean. Quat. Sci. Rev. 143, 84–95.
Ramos-Román, M.J., Jiménez-Moreno, G., Camuera, J., García-Alix, A., Anderson, R.S., Jiménez-Espejo, F.J., Carrión, J.S., 2018a. Holocene climate aridification trend and human impact interrupted by millennial and centennial-scale climate fluctuations from a new sedimentary record from Padul (Sierra Nevada, southern Iberian Peninsula). Clim. Past 14, 117–137.
Ramos-Román, M.J., Jiménez-Moreno, G., Camuera, J., 2018b. Millennial-scale cyclical environment and climate variability during the Holocene in the western Mediterranean region deduced from a new multiproxy analysis from the Padul record (Sierra Nevada, Spain). Glob. Planet. Chang. 168, 35–53.
Ramos-Román, M.J., Jiménez-Moreno, G., Anderson, R.S., García-Alix, A., Camuera, J., Mesa-Fernández, J.M., Manzano, S., 2019. Climate controlled historic olive tree occurrences and olive oil production in southern Spain. Glob. Planet. Chang. 182, 102996.
Rasmussen, S.O., Andersen, K.K., Svensson, A.M., Steffensen, J.P., Vinther, B.M., Clausen, H.B., Siggard-Andersen, M.-L., Johnsen, S.J., Larsen, L.B., Dahl-Jensen, D., Bigler, M., Röthlisberger, R., Fischer, H., Goto-Azuma, K., Hansson, M.E., Ruth, U., 2006. A new Greenland ice core chronology for the last glacial termination. J. Geophys. Res. 111, D06102.
Reimer, P.J., Austin, W.E.N., Bard, E., Bayliss, A., Blackwell, P.G., Bronk Ramsey, C., Butzin, M., Cheng, H., Edwards, R.L., Friedrich, M., Grootes, P.M., Guilderson, T.P., Hajdas, I., Heaton, T.J., Hogg, A.G., Hughen, K.A., Kromer, B., Manning, S.W., Muscheler, R., Palmer, J.G., Pearson, C., van der Plicht, J., Reimer, R.W., Richards, D.A., Scott., E.M., Southon, J.R., Turney, C.S.M., Wacker, L., Adophi, F., Büntgen, U., Capano, M., Fahrni, S., Fogtmann-Schulz, A., Friedrich, R., Kudsk, S., Miyake, F., Olsen, J., Reinig, F., Sakamoto, M., Sookdeo, A., Talamo, S., 2020. The IntCal20 Northern Hemisphere radiocarbon calibration curve (0–55 cal kBP). Radiocarbon 1–33.
Renssen, H., Brovkin, V., Fichefet, T., Goosse, H., 2003. Holocene climate instability during the termination of the African Humid Period. Geophys. Res. Lett. 30, 1184.
Rodrigo-Gámiz, M., García-Alix, A., Jiménez-Moreno, G., Ramos-Román, M.J., Camuera, J., Toney, J.L., Sachse, D., Anderson, R.S., Damsté, J.S.S., 2022. Paleoclimate reconstruction of the last 36 kyr based on branched glycerol dialkyl glycerol tetraethers in the Padul palaeolake record (Sierra Nevada, southern Iberian Peninsula). Quat. Sci. Rev. 281, 107434.
Rodrigo-Gámiz, M., Martínez-Ruiz, F., Rampen, S.W., Schouten, S., Sinninghe Damsté, J. S., 2014. Sea surface temperature variations in the western Mediterranean Sea over the last 20 kyr: a dual-organic proxy (UK′37 and LDI) approach. Paleoceanogr. 29, 87–98.
Rubiales, J.M., García-Amorena, I., Hernández, L., Génova, M., Martínez, F., Gómez Manzaneque, F., Morla, C., 2010. Late Quaternary dynamics of pinewoods in the Iberian Mountains. Rev. Palaeobot. Palynol. 162, 476–491.

Shen, Y., Sweeney, L., Liu, M., López Sáez, J.A., Pérez-Díaz, S., Luelmo-Lautenschlaeger, R., Gil-Romera, G., Hoefer, D., Jiménez-Moreno, G., Schneider, H., Prentice, I.C., Harrison, S.P., 2022. Reconstructing burnt area during the Holocene: an Iberian case study. Clim. Past 18, 1189–1201.

Simón, M., Sánchez, S., García, I., 2000. Soil-landscape evolution on a Mediterranean high mountain. Catena 39 (3), 211–231.

Toney, J.L., García-Alix, A., Jiménez-Moreno, G., Anderson, R.S., Moossen, H., Seki, O., 2020. New insights into Holocene hydrology and temperature from lipid biomarkers in western Mediterranean alpine wetlands. Quat. Sci. Rev. 240, 106395.

Van Geel, B., Coope, G.R., van der Hammen, T., 1989. Palaeoecology and stratigraphy of the Lateglacial type section at Usselo (The Netherlands). Rev. Paleobot. Palynol. 60, 25–129.

Valle, F., 2003. Mapa de series de vegetación de Andalucía 1: 400.000. Editorial Rueda.

Walker, M., Head, M.J., Berkelhammer, M., Björck, S., Cheng, H., Cwynar, L., Fischer, D., Gkinis, V., Long, A., Lowe, J., Newham, R., Olander Rasmussen, S., Weiss, H., 2018. Formal ratification of the subdivision of the Holocene Series/Epoch (Quaternary System/Period): two new Global Boundary Stratotype Sections and Points (GSSPs) and three new stagers/subseries. Episodes 41 (4), 213–223.

Zamora, R., Oliva, M., 2022. The landscape of the Sierra Nevada. Springer Nature Switzerland AG.